Advances in Thermal Processes and Energy Transformation
Volume 3, 2020, HOCK02, pp. 58-64
ISSN 2585-9102

Transformation of an Aviation Turboshaft Engine into a Gas Turbine Experimental Facilities for Laboratory Testing

Marián Hocko[1]

[1]*Faculty of Aeronautics, Technical University of Košice, Rampová 7, 042 21 Košice, Slovakia, e-mail: marian.hocko@tuke.sk*

Category: Original Scientific Paper
Received : 21 September 2020 / Revised: 24 October 2020 / Accepted: 25 October 2020

Keywords: Experimental Verification of Unstable Work of a Radial Compressor, Unstable Work of Compressor, Small Experimental Turbojet Engine MPM-20, Turboshaft Engine,

Abstract: The article deals with the use of a small aviation turboshaft engine for laboratory purposes. This study describes its transformation into an experimental device for research and education. Various constructional, technological and controlling modifications and settings of the gas turbine test stand were carried out and tested on a stationary configuration. The stationary system can be used as a small backup power generator or as a drive unit for a compressor, pump, etc. The laboratory equipment can also be used for research into biofuels (fatty acid methyl esters and bioethanol) for use in aviation and energetics. New control systems, electronic elements and methods of measuring rotations, pressure and temperature are tested for educational and research purposes. The study includes a schematic description of modelling measurements and subsequent numerical evaluation of the thermodynamic characteristics of the cycle in an experimental gas turbine. The laboratory device presented here is, thanks to technological, material and thermodynamic research, suitable for educating and testing the knowledge of future aviation and mechanical engineers.

Citation: Hocko Marián: Transformation of an Aviation Turboshaft Engine into a Gas Turbine Experimental Facilities for Laboratory Testing, Advance in Thermal Processes and Energy Transformation, Volume 3, No. 3, (2020), p. 58-64, ISSN 2585-9102

1 Introduction

Unstable work (surge) of compressors is a dangerous phenomenon that occurs in a particular mode of compressors of aviation turbo-compressor engine (ATCE) and also gas turbine (GT) that are used in vehicles and stationary applications. That is manifested by sudden changes in pressure and speed of the airflow at the outlet of the compressor and by characteristic sound effects that give rise to intense vibrations of the rotor blades and by changes of the of air flow characteristics in other parts of both ATCE and GT. The consequences of unstable work of the compressor are associated with cessation of activities of ATCE and GT, or their destruction because of mechanical damage of the compressor blades or destruction (burning) of the gas turbine blades. Therefore, the formation of unstable work of the compressor is inadmissible and much attention is devoted to prevention of its starting in ATCE and GT.

Carrying out the research in unstable work of ATCE and GT compressors in a real operational context is associated with potential security risks and significant economic costs due to damage or destruction of expensive engines. Relevant results can be achieved without the mentioned risks under the laboratory conditions using the experimental small turbojet engine MPM-20 that was created by transforming the turbine trigger TS-20 into a small single jet engine. In experiments conducted at the Department of Aviation Engineering at the Faculty of Aeronautics, Technical University of Kosice, artificially induced unstable work of a centrifugal compressor, virtually confirmed the hypotheses and the relevant consequences for particular parts of the engine [1].

2 Launch Mechanism of Unstable Compressor Work

Unstable work of the ATCE compressor is a phenomenon that occurs when a particular mode of work of the compressor is manifested by severe periodic changes in the air flow rate Q_{Air}, the output pressure p_2 and absolute air speed can sometimes back-

flow of air from the compressor to the input ATCE device.

Concomitants of unstable work of the ATCE compressor are:

- pulsation of pressure and air velocity at the outlet of the compressor,
- a reduction of the mean pressure at the outlet of the axial compressor $p_{2m.}$
- characteristic sound effects,
- engine vibration,
- vibration of compressor rotor blades.

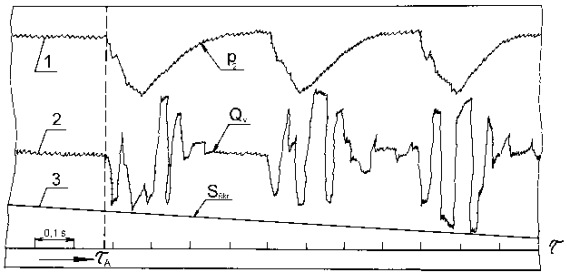

Figure 1 Recorded parameter changes as the compressor is in surging [2]
1 - course of changes in output static pressure p_2, 2 - course of changes in air flow Q_{Air} through the compressor, 3 - change of the active cross-section flow $S_{škr.}$ through the compressor

The formation of unstable compressor work during the operation of ATCE or GT can occur for various reasons, for example as a consequence of:

- unstable work of input ATCE or GT device,
- failures of an engine control system (accelerator machine, high-pressure pump, etc.),
- sucking an object (birds, ice, etc.),
- sudden changes in temperature conditions at the inlet to the engine (while passing over the fire, active volcano or sucking the off-gasses of another aircraft or launched missiles, etc.),
- sudden changes in active areas of the input device of the engine when aircraft is maneuvering,
- changes in air quality, for example in sucking volcanic ash volcanic when flying in the volcanic cloud and the like.

The consequence of unstable work of the ATCE or GT compressors can be:

- an irregular operation of the engine,
- a reduction in thrust (power) owing to reduced flowing amount of air through the engine,
- distortion of the normal steady burning of fuel-air mixture in the main combustion chamber of ATCE,
- the sharp increase in gas total temperature in front of the gas turbine ATCE T_{3t},
- increase of the vibration level of the whole ATCE,
- possibility of breakage of the ATCE compressor rotor blades because of vibration.

Regarding the accompanying phenomena, which may lead to an interruption of the engine, its damage, or destruction of unstable work of the compressor, is admissible [5].

The entire process of creating the unstable work of the ATCE compressor is rather complicated. The physical principle to form unstable compressor work is based on tearing streamlines of airflow at the run around an individual compressor blade when major departure from the calculation mode of operation of the compressor, resulting in a sudden change in the air supply and pressure conditions at the inlet of the compressor ATCE.

3 Launch of Unstable Compressor Work of an Axial Compressor

In operation, the axial compressor in a computing mode corresponds to the air flow rate $Q_{Air} = Q_{Air,cal.}$ of the rotor speed n and the peripheral speed of the rotor u_1 at the absolute inlet air velocity c_1 specifies the initial relative air speed at the rotor blade inlet w_1, which flows in the direction of a tangent towards the central curve profile of a rotor blade to in between rotor blade channel. The outlet absolute velocity of the air from the compressor rotor blade c_2 enters in between a rotor blade channel in the direction of a tangent towards the curve profile of a central stator vane. The airflow through the axial compressor stage is smooth, without creating turbulence. The axial compressor is stable (Figure 2a).

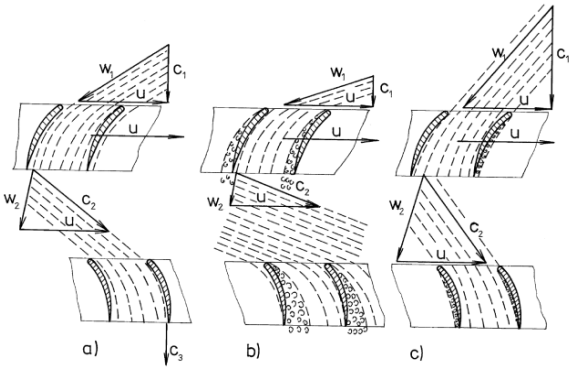

Figure 2 The airflow character of an axial compressor stage

In reducing the rate of airflow $Q_{Air} < Q_{Air,\ cal}$ and particular engine speed n, the circuit rotor speed u will create, with reduced absolute speed $c_{1,}$ the resulting relative speed w_1 the direction of which will deflect from the tangent to the medium curve of a rotor blade profile. This disrupts the smooth rotor blade and on their backs tearing off streamlines will occur and laminar flow to turbulent flow will be converted and spread farther to the stator vanes and other stages of the axial compressor. The roiled air flow in an axial compressor reduces smooth air flow farther into the main ATCE combustion chamber; it will result in backward flow of air back towards the ATCE input device. So the back flow of air in the space in front of

the main combustion chamber sharply reduces air pressure and the air starts to move away from the input device to the main ATCE combustion chamber. The unstable air flow (surge) through the ATCE axial compressor results in an abrupt change in the composition of the fuel-air mixture in the main combustion chamber which causes a significant increase in the overall total temperature of the gas in front of the gas turbine T_{3t} (sparingly rich mixture of fuel and air) and vibration of the rotor blades of the axial compressor with the possibility of their damage due to fatigue fracture (Figure 2b).

With an increase in the rate of airflow $Q_{Air} > Q_{Air,cal.}$, and the particular rotor speed n the circuit rotor speed u will create, with the increased absolute speed $c_{1,}$ a resulting input relative velocity of the air at the entrance to the rotor blades w_1 the direction of which will deviate from the direction of the tangent to the profile middle curve of the rotor blade. This will cause hindering the smooth laminar airflow in the riverbed of rotor blades. The turbulent flow in the riverbed of blades will decline and there will be no farther spread of the breakaway streamlines into other stages of the axial compressor. Therefore, in this case there will be no formation of unstable work of the ATCE axial compressor (Figure 2c).

4 Launch of Unstable Compressor Work of a Radial Compressor

Unstable work of the ATCE radial compressor results from tearing of the air flow to the impeller blades and the vanes of the diffuser at larger angle of attack changes in the incoming air, which may be caused by changing of the air flow rate, or by changing the rotor speed of the compressor.

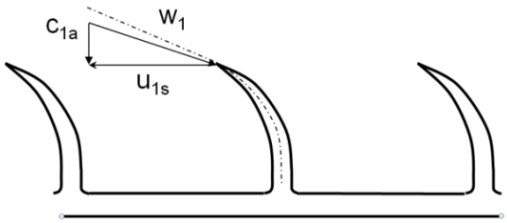

Figure 3 Stable air flows of radial compressor blades

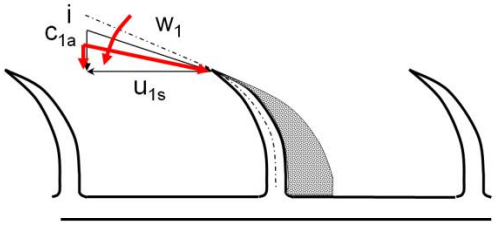

Figure 4 Unstable air flows of radial compressor blades

The formation of unstable work of the ATCE centrifugal compressor usually occurs at higher values of calculated speed n_p, such as computing speed mode $n_{p,cal.}$.

$$n_p = n.\sqrt{\frac{288}{T_1.\left(1+\frac{\kappa-1}{2}.M_1^2\right)}}\ [\min.^{-1}] \quad (1)$$

Where:
n_p - converted speed [min^{-1}],
n - measured speed of rotation [min^{-1}],
T_{1t} - the total air temperature at the inlet to the radial compressor [K],
T_1 - static air temperature at the inlet to the radial compressor [K],
M - Mach flight number [1].

The equation (1) shows that the calculated speed will increase at low static air temperature T_1 and low speed expressed in the figure M_1, corresponding to activities of ATCE in climbing to a great height.

If the air flow rate through a radial compressor equals to the computational rate of air flow $Q_{Air} = Q_{Air,cal.}$, the airflow of radial compressor blades and diffuser vanes is smooth, the unstable work of a radial compressor will not occur. The radial compressor will work stably (Figure 3).

If the air flow rate through a radial compressor is greater than the calculated air flow rate $Q_{Air} > Q_{Air,cal.}$ tearing off the air flow in the riverbed of a radial compressor blades will occur. As the tearing area of the air flow is relatively small, it does not spread. On the diffuser vanes the air flow is tearing off on the back of the blades. Air particles tend to move along the curves that are close to the logarithmic spirals. Rolling of the air flow reduces the efficiency of radial compressor, but the air stream flows through the radial compressor but unstable work of the compressor usually does not occur (Figure 5).

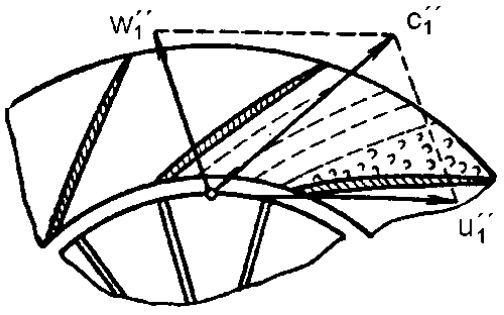

Figure 5 Tearing off the air streamlines on the back of diffuser vanes at $Q_{Air} > Q_{Air,cal.}$.

In reducing the rate of air flow through a radial compressor below the calculated amount of air $Q_{Air} < Q_{Air,cal.}$, tearing off the airflow at the back of the impeller blades (Figure 4) and diffuser vanes will

occur (Figure 6). The detached air stream loses velocity and reduces the flow area. So the decrease in the kinetic energy tends to increase the static pressure, which leads to the return flow and the consequent restoration of steady flow (surge). This process is again repeated at short intervals [2, 3].

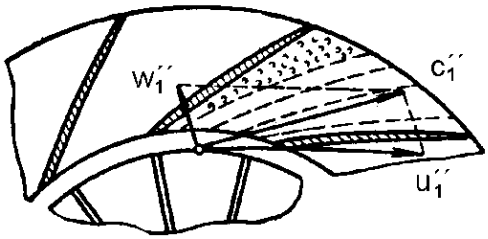

Figure 6 Tearing off the air streamlines on the back of diffuser vanes at $Q_{Air} < Q_{Air,cal.}$

5 Experimental Verification of Unstable Work of a Radial Compressor

As mentioned in the previous part of this article, one of the causes of ATCE compressor unstable work is a change of air flow through the engine inlet device as a result of throttle down from variety of reasons. In theory, this process is explained in the particular (constant speed) mode by shifting an operating point along the linen = const. in the characteristics of a radial compressor to the left border of the unstable work [4]. In sufficient reduction in air flow rate Q_{Air} via the input device the operating point of the engine exceeds a threshold of unstable work and gets in unstable work of the radial compressor (surge area) (Figure 7).

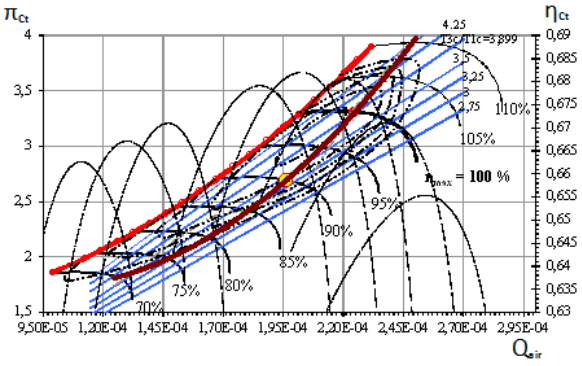

Figure 7 Calculated characteristics of a radial compressor of an experimental small turbojet engine MPM-20

For practical testing of the theoretical hypotheses, the Laboratory for small turbojets at the Department of Aviation Engineering, Technical University of Kosice has been used, in which the experimental small single jet engine is available, it was created by conversion of the turbine trigger TS-20 [7].

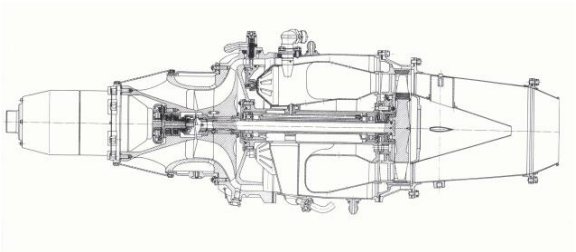

Figure 8 Section of a small turbojet engine MPM-20

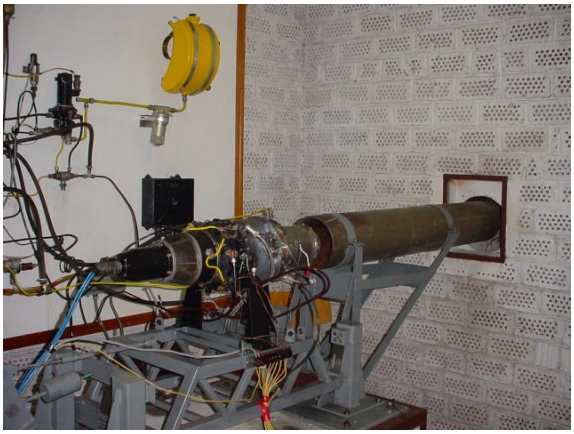

Figure 9 View of the MPM-20 at the Laboratory of small jet engines

6 Throttling of Airflow in the Inlet System

The practical experimental verification of the impact of throttling the flow of air in the intake device of MPM-20 on an unstable work of a radial compressor, the method for gradual increasing the density of nets has been implemented; each was placed on the input system of the engine.

The processed linear mathematical model of MPM-20 is based on the theory of small changes in [8], described in [1, 10] for the sub-critical conditions of flow in the outlet nozzle, defines the conditions of change in the intake device reflected by changes of all parameters of the working process of single jet ATCE. For practical validation of this theory four sets of experimental measurements were prepared and aimed at gradually throttling the air flow through the input device MPM-20th. The measured parameter values for individual experimental measurements are compared with the values obtained in the calibration measurement and the theoretical calculation based on the theory of small changes. Gradually these experimental measurements were realized:

1. Air flow through the input device of MPM-20 without the input sieve.
2. Air flow through the input device of MPM-20 with the sieve mesh size of 1.5 x 1.5 mm.

3. Air flow through the inlet system of MPM-20 with the double sieve (the sieve with a mesh size of 1.5 x 1.5 mm and the sieve with mesh of 2.5 x 2.5 mm).
4. Air flow through the inlet device of MPM - 20 with a TV viewing screen with openings with a diameter of 0.4 mm.

The change in the independent variable (failures) was calculated according to the formula:

$$\delta X_{si} = \left[\frac{X_{si} - X_0}{X_0} \right].100[\%] \qquad (2)$$

where:
δX_{si} – change in the independent variable,
X_{si} – a value parameter in a simulated mal function,
X_0 – an original value of the independent variable.

The change in the dependent variable value was calculated according to the equation:

$$\delta Y_{si} = \left[\frac{Y_{si} - Y_0}{Y_0} \right].100[\%] \qquad (3)$$

where:
δY_{si} – a change of the dependent variable,
Y_{si} – a value parameter in the simulated malfunction,
Y_0 – an original value of the dependent variable.

6.1 The Airflow through the Inlet Device of MPM-20 without an Inlet Sieve

For the conditions of the first experiment the original input protective sieve was removed from the entrance system of MPM-20.

Before carrying out the planned experiments, the MPM-20 was set according to the technical documentation for a calculation scheme [9]. Subsequently 10 measurements of calibration parameters were performed. The mean value of the measured parameters obtained by the calibration measurement served as a bench mark for assessing changes in subsequent experimental measurements.

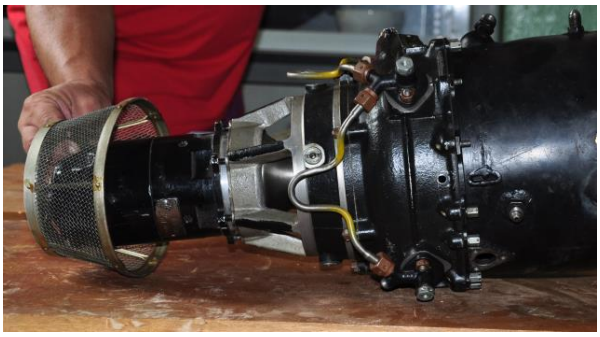

Figure 10 Removing the protective sieve from MPM-20

Table 1 Comparison of calculated and measured values of the parameters in the calibration measurements of MPM–20

PARAMETER	p_H	T_H	ACTIVITY PERIOD	$p_{2,C}$	$p_{2,C}$	p_{2t}
UNIT	**Pa**	**K**	**second**	**Pa**	**Pa**	**Pa**
MEASURED VALUE	99885,82	290,65	50,8	180787,9	392652,7	351971,5
COUNTED VALUE	101325,2	288	50	181600,13	398549,2	392321,5
PARAMETER	p_3	p_4	T_{2t}	T_{2t}	T_{3t}	T_{4t}
UNIT	**Pa**	**Pa**	**K**	**K**	**K**	**K**
MEASURED VALUE	351326,2	154655,78	458,55	460,25	1170,35	1043,45
COUNTED VALUE	392321,5	162812,95	462,35	462,35	1168,15	1013,27
PARAMETER	Q_{fuel}	G_{fuel}	c_h	F_T	G_{AIR}	c_m
UNIT	$cm^3/_{CYCLE}$	$kg/_{CYCLE}$	$kg.h^{-1}$	**N**	$kg.s^{-1}$	$kg.h^{-1}.N^{-1}$
MEASURED VALUE	1362	1,05572	74,87	-	-	-
COUNTED VALUE	-	-	-	698,09	1,2	0,1311

A relatively high degree of agreement of measured and calculated thermodynamic parameters is apparent from the results of the calibration measurements processed in MPM-20 and its comparison with the results of thermodynamic calculation of heat circulation of MPM-20. Minor deviations between measured and calculated values of the thermodynamic parameters are caused by irregularities occurring in the measurement because of the location of sensors in other positions as suggested in the theoretical calculation.

In the first experiment (Figure 10) 10 measurements were performed and the same parameters as for the calibration measurements MPM-20 in the original configuration (with a protective sieve) were measured and evaluated. The mode of MPM-20 operations was set to values that correspond to the calibration measurement (computing) mode; external conditions (p_H, T_H) have not changed.

As is apparent from the data given in [1], that compares the measured values of the parameters in the experimental measurements without the input sieve and the calibration measurements, the differences in individual parameters are minimum and range from -5.4 % (static gas pressure for gas turbine p_4) to +2.9 % (total gas temperature for gas turbine T_{4t}). Most of the other observed parameters have hardly changed even though the flow area of the inlet to the MPM-20, after the removal of the inlet sieve, grew by 35 % (a total area of the inlet sieve with a wire sieve of a mesh size of 2.5 x 2.5 mm and wire thickness of 0.6 mm wire is 0.078593 m^2).

The results obtained by direct measurement of MPM-20 without input sieve confirm that the choice of the wire diameter and the mesh size has been optimized by the engine manufacturer so that the sieve provides the protection from sucking strange objects with a minimum influence on the parameters of MPM-20. Based on the measured parameters, the calculation of thrust F_T and of specific fuel consumption c_m were performed.

6.2 The Airflow through the Inlet Device of MPM- 20 with the Soft Inlet Sieve

In the second experimental measurement, the air flow through the soft sieve of an input device was throttled, which was deployed on the input device of MPM-20. The total area of the inlet sieve is 0,078593 m^2. When using a wire sieve with a mesh size of 1.5 x 1.5 mm and at thickness of 0.3 mm wire, the occupied area of the input wire sieve is 34.984 % of the total area of the input device. The measured values of parameters of MPM-20, described in [1], are very close to the measured values in calibration measurements with the original sieve.

6.3 The Airflow through the Inlet Device of MPM-20 with the Double Inlet Sieve

Third, experimental measurements were carried out at throttling off low with the dual sieve (Figure 11). To the original input device with an original protective sieve of MPM-20 a soft sieve with the mesh size of 1.5x1.5 mm and a thick ness of 0.3 mm wire was deployed, thus reducing the flow a real by 58 %. On the basis of the reduction in the flow area of the inlet system the measured thermodynamic parameters have been changed, resulting in a change of the engine-dependent parameters. The total degree of gas expansion significantly changed on the gas turbine π_{Tt} (about 19.194%) and the total temperature of gas behind the gas turbine T_{4t} (by 4,475%).

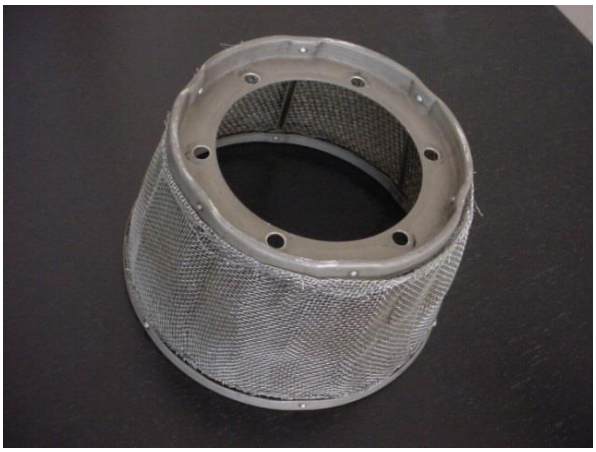

Figure 11 Dual sieve of MPM-20

6.4 Airflow through the MPM-20 input system with the finest inlet sieve

Figure 12 Perforated plates attached to the original inlet device of MPM-20

The recent experimental measurement was carried out with strong throttling of flow through the input device, using a perforated metal plate with round holes 0.4 mm (a metal plate was originally used as a color TV viewing screen) (Figure 12, 13). The perforated plate was placed on the original sieve of an input device, thereby allowing a reduction by 83 % in the flow area of the inlet system of MPM-20. This reducing of the flow are of the engine inlet device was substantial degradation of measured parameters compared to measured parameters at the input device without the inlet sieve (Δp_{2t} = -48 978,8 Pa, Δp_3 = 24 198,5Pa, Δp_4 = -24 957,82Pa, T_{2t} = -11,6K, ΔT_{3t} = -92,4K, ΔT_{4t} = -177,5 K, c_h = -4,3465kg.h^{-1}, $\Delta\pi_{Tt}$ = 0,6, $\Delta\pi_{Ct}$ = -0,509 a $\Delta\pi_{exh.}$ = -0,257.

The seventh measurement with 83 % shading of the input device was in an unstable work of a radial compressor of the engine and the destruction of gas turbine blades and to burn the sealant mass in the body of the gas turbine above rotor blades (Figure 13, 14).

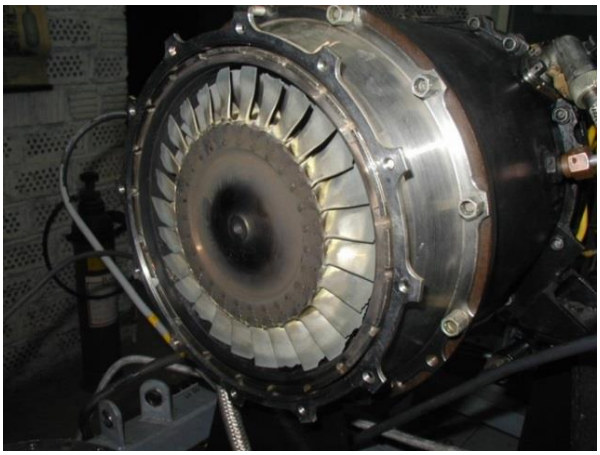

Figure 13 Destroyed gas turbine rotor blades of MPM-20 because of unstable work of a radial compressor

Figure 14 Tanned seal in gas turbine housing

7 Conclusions

Throttling of an input device of MPM-20 changes parameters in the engine, their character is the same as the change in a coefficient of maintaining the total air pressure in the intake device σ_{int}.

The throttling of the inlet device of MPM-20, from the thermodynamic parameters, mostly effects the static pressure of the gas behind the gas turbine p_4 (-19.39 %), the total temperature of the gas behind the gas turbine T_{4t} (-17.081 %), total air pressure behind the compressor p_{2t} (- 13.95 %), total gas pressure the in front of the gas turbine T_{3t} (-7.903 %) and a total air temperature behind the compressor T_{2t} (-2.524 %).

Throttling input device MPM-20 leads to a higher operating point convergence to the limit in the characteristics of unstable labor centrifugal compressor.

Despite higher resistance of the radial compressor of MPM-20 comparing to against unstable work was the seventh measurement with 83 % throttling of the inlet system to its unstable work and destruction of gas turbine blades and burn of the sealant mass in the body of the gas turbine above the rotor blades.

Changing of the inlet flow cross-section to the ATCE and GT radial compressors has a significant effect on its thermodynamic and performance parameters. When in case of large throttling or sudden reductions in air flow through the input device, unstable flow may affect a specific area or the entire radial compressor, which may cause damage to the ATCE gas turbine (Figure 13, 14).

Table 1 Comparison of calculated and measured values of the parameters in the calibration measurements of MPM–20

PARAMETER	$S_{inlet.}$	p_H	T_H	Activity period	$p_{2,c}'$	$p_{2t,c}'$
UNIT	%	Pa	K	second	Pa	Pa
Inlet device without a sieve	100	100525,3	288,75	51,0	178967,1	388941,8
Inlet device with a soft sieve	80	100365,6	290,95	49,7	179136,7	390028,1
Inlet device with a basic sieve	65	99885,82	290,65	51,7	180787,9	391185,7
Inlet device with a dual sieve	58	100125,3	290,65	49,7	198319,4	397633,7
Inlet device with the softest sieve	17	99991,98	290,29	50,0	213852,3	428407,3
PARAMETER	p_{2t}	p_3	p_4	T_{2t}'	T_{2t}	T_{3t}
UNIT	Pa	Pa	Pa	K	K	K
Inlet device without a sieve	351178,4	351524,7	128716,5	458,35	459,55	1169,25
Inlet device with a soft sieve	351571,5	351462,6	128977,1	458,45	459,95	1170,05
Inlet device with a basic sieve	351971,5	351326,2	154655,8	458,55	460,25	1170,35
Inlet device with a dual sieve	366122,2	340125,3	154192,9	460,65	461,95	1172,95
Inlet device with the softest sieve	400157,2	327326,2	153674,3	470,01	471,15	1261,65
PARAMETER	T_{4t}	Q_{fuel}	G_{fuel}	c_h	F_T	c_m
UNIT	K	cm^3/cycle	kg/cycle	$kg.h^{-1}$	N	$kg.h^{-1}N^{-1}$
Inlet device without a sieve	1039,15	1407	1,09045	77,0065	732,5	0,1051283
Inlet device with a soft sieve	1041,15	1405	1,0889	78,8700	731,6	0,107811
Inlet device with a basic sieve	1043,45	1397	1,0819	75,2900	698,1	0,107847
Inlet device with a dual sieve	1085,65	1330	1,0312	74,7434	598,74	0,125334
Inlet device with the softest sieve	1216,65	1293,3	1,0027	72,6600	541,11	0,13428

The reference list

[1] HOCKO, M.: *Assessment of the ATCE State Based on Changes in Thermodynamic Parameters*, thesis, pp. 338, 2003.

[2] RUZEK, J.: *Theory of Aircraft Engines, Part I (Compressors, Turbines and a Combustion Chamber),* pp. 373, University textbook VA AZ Brno, 1979.

[3] OTT, A.: *Fundamentals of the Theory and Design of Air Vane Engines, Part I*, University Textbook, pp.140, Military Academy of Aviation, Kosice, 1983.

[4] MED, S.: *Diagnosis of JE - TS-20 in Laboratory Conditions K – 316*, master's thesis, Department of Aircraft, Military academy in Brno, 1999.

[5] CUMPSTY, N.A.: *Compressor aerodynamics*, Department of Engineering University of Cambridge, pp. 687, 1989.

[6] HOCKO, M., GASPAR, R.: *Impact of rapid thermal fluctuations of the air flow into engine inlet to the gas-dynamics stability of the turbojet engine*, 12th conference Power System Engineering, Thermodynamics & Fluid Flow, Pilsen, pp. 8, 2013.

[7] HOCKO M.: *The small jet engine MPM-20*, VLA Kosice, 2003.

[8] ČERKEZ, A.J.: Инжинерные расчеты газотурбиных двигателей методом малых одклонений, *(Engineering calculations of gas turbine engines by the method of small deviations),* Издательство Машиностроиение (Publishing house Mashinostroenie), pp. 379, 1975.

[9] The operation and maintenance of the engine AL-7F-1, Book 2, Book 3, Let -21 -20/2, Let -21 -20/3, Praha 1965.

[10] FŐZŐ, L., ANDOGA, R., MADARÁSZ, L., Mathematical model of a small Turbojet Engine MPM-20, *Studies in Computational Intelligence*, Vol. 313, p. 313-322, 2010.

Advances in Thermal Processes and Energy Transformation
Volume 3, 2020, MIHA01, pp. 65-70
ISSN 2585-9102

The Aspects of Research and Education Activities in the Field of Renewable Energy Carriers

Ján Sarvaš[1] ● Michal Zubko[1] ● Daniela Hrbková[1] ● Tomáš Vaško[1] ● Janka Mihalčová[1]

[1]*Research and education centre of bioenergy, University of Economics in Bratislava, 08212 Kapušany, Slovakia, e-mail: janka.mihalcova@gmail.com*

Category : Professional Paper
Received : 21 July 2020 / Revised: 24 August 2020 / Accepted: 25 August 2020

Keywords : analysis, biogas plant, biomass, education, renewable energy, research, sustainable growth

Abstract : Energy politics of Slovakia is focused on sustainable economic growth and competitiveness by the means of sustainable Slovak energetics. The increase share of renewable energy carriers in the production of electricity and heat leads to a reduction in the consumption of fossil fuels and that consequently contributes to the reduction of pollutants and greenhouse gases. The existing regional potentials in the field of electricity and heat production are in the form of renewable energy carriers and the largest contributor is biomass. The development of the use of alternative energy sources aro uses a need for researchand development as well as new qualified professionals. The support from the European Union has enabled to build a work space that combines research and development activities with the processes of education and training and therefore is creating the conditions for the training of the professionals and the promotion of ideas in the field of renewable energy carriers.

Citation: Sarvaš Ján, Zubko Michal, Hrbková Daniela, Vaško Tomáš, Mihalčová Janka: The Aspects of Research and Education Activities in the Field of Renewable Energy Carriers, Advance in Thermal Processes and Energy Transformation, Volume 3, No.3, (2020), p. 65-70, ISSN 2585-9102

1 Introduction

The use of renewable energy carriers (REC) is based on advanced and environmentally friendly technologies which leads to a reduction in greenhouse gas and pollutant emissions. The Green Report 2018 states that thein crease in the number of built biogas plants (BPS) has been stagnating in there cent period. The most BPS have an installed capacity in the range of 0,9 – 1,0 MW and most of them are focused on the production of electricity from corn silage. The consumption of corn silageinto BPS in Slovakia has, according to expert estimate, reached 1,2 mil. tons per year. The construction of other BPS and thus an other corn consumption on a biogas production could endanger the stocks of bulk feed for animal production. There foreit will be necessary, when building new BPS in Slovakia, to focus on the processing of other forms of biomass, as invasive plants, bio-waste etc. [1, 2]. The strategical aim of the Energy Policy of the Slovak Republic which was approved pursuent to the Slovak Government resolution No 548/2014 is to achieve competitive low-carbon energy which would provide safe, reliable and efficient supply of all energy forms at affordable prices considering consumer protection and sustainable development. It defines key objectives and priorities of energy sector until 2035 with a long-term time horrizon until 2050. The concept of the energy development is focused on the optimization of energy mix from the point of view of energy security. The emphasis is laid on the use of domestic energy sources and low-carbon technology, as renewable sources and nuclear energy. From the point of view of the structure of the used primary energy sources, the Slovak republic has a balanced share of individial energy sources in gross inland consumption. The Slovak energy mix has a balanced share of nuclear fuel and fossil fuels in gross inland consumption. [3] Slovakia agreed to international conventions in the field of air, ozone layer and climate protection and has been meeting the obligations arising from it. The use of renewable energy sources is growing dynamically, since 2001 it has increased from 30PJ for consumption in 2012 to 59 PJ. In Slovakia the greatest energy potential among renewable energy sources (RES) has

biomass with a theoretical potential of 120 PJ. The Slovak Republic is obliged to increase the use of RES in relation to gross final consumption of energy - from 6,7 % in 2005 to 14 % in 2020 and to achieve the use of RES at the level of 80PJ in 2020 and 120PJ in 2030. The increase of the share of RES in energy and heat production in order to create adequate additional sources needed to cover domestic demand is one of the main priorities of the Energy Policy of the Slovak Republic [4, 5]. The link between the education system with the needs of the labour market is a strategical aim of the Slovak Republic and it requires inreasing of the involvement of employers in the creation and innovation of educational content. The central field is the support of vocational education and the creation of the link between studies and practice. Concerning higher education, it is also needed to strenghten quality and content of bachelor´s degree in order to ensure the needs of practice in accordance with the objectives of National Strategy for Smart Specialization of the Slovak Republic RIS3 SK. The creation of bachelor and engineering programmes more focused on jobs in the field of energetics with respect to the use of alternative sources of bioenergy. Within the conception of support of the cooperation with practice a centre of university cooperation was established . Its task is to support research cooperation of university facilities with practice and to ensure the direction of private-sector investment in research and education and to support science and technology education for the needs of industry and practice. The effort is to help and convince the society as well as put into practice the idea of using renewable energy carriers. To initiate and give instructions for businessmen and minicipalities how to use yet undiscovered existing regional potentials of renewable sources of energy, as biomass, geothermal and hydro energy and waste [6, 7].

2 Research and Education Centre of Bioenergy

Research and education centre of bioenergy (RECB) was established on the basis of the implementation of an applied project in 2007 as an EU workplace based in Kapušany. Its purpose is research and development in the field of extraction and recovery of biomass and solar energy and their efficient use for energy purposes in business practice. Also improvement of the education process and knowledge and experience production in the development of the conditions of sustainable development in disadvantaged Slovak regions. With the support of the project from the European Structural Funds, the RECB has become a centre of cooperation with practice in the field of renewable energy carriers since 2007. It is situated in the area of the agricultural cooperative Kapušany near Prešov. It is therefore directly connected with practice, it fullfils the function of an integrating and coordinating organisational unit, while it creates the conditions for the use of the latest knowledge in the field of renewable energy carriers in practice in the cooperation with the University of Economics in Bratislava and The Technical University of Košice [8].

One of the essential tasks of the center within the following science and research project is to optimalise the activity of the biogas plan in agricultural cooperative Kapušany which makes use of agricultural products and waste and was built in 2002 (Figure 1). It was an older type of biogas station with technical and operational shortcomings and thus it showed only 50% efectiveness in the conversion of primary energy (biomass and slurry), which accounts for 70 to 100 kWh of the electricity produced. The goal of the project was to increase the efficiency of fermentation and cogeneration processes of the biogas plant. The project was focused on the preparation and replenishment of inputs and the conversion of the substrates in an anaerobic digestion process to produce biogas and their use by the cogeneration process to produce electricity and heat. The optimal performance of this biogas plant should be around 170 to 180 kWh of the produced energy. The fermentation process is strongly influenced by the input which is mostly corn silage. The homogenization to the right size, heat treatment and constant dose are necessary to be done. This is ensured by a homogenizer and a substrate dispenser. The temperature and pressure at the inlet and outlet of the fermentor are being monitored, which are important factors for a proper operation and potencial identification of problems with the operation of the biogas plant. The properties of already generated biogas are regularly monitored before the inlet to the cogeneration unit by the means of content analyzer CO_2, O_2, CH_4 a H_2S.

Figure 1 Biogas plant in the agricultural cooperative Kapušany near Prešov

3 Research and Education Activity of RECB

The workplace is focused on the solutions of the scientific and technical projects as well as grants in the

field of renewable energy sources and the modernization of already existing energy facilities, especially biogas plants, in order to increase their efectiveness. It is directed at authentication and application of the research outcomes into common practice which creates space for the cooperation with entities dealing with the evaluation of alternative energy sources in practice. The workplace also serves as a counseling and information centre for those who are interested in using alternative sources.

In addition to research in the field of renewable energy carriers, the Research and Education Centre of Bioenergy (RECB) is also involved in education and awareness-raising on energy and renewable energy sources (RES). There are two seminar rooms with computer equipment and the possibility to make presentations and visualizations of renewable energy carriers processes (Figure 2). The workplace provides additional education and professional practice for students on the latest knowledge in the field of renewable energy sources and their use in practice. It provides excursions for primary and secondary school students with demonstrations of solutions for the use of new technologies for energetically, environmentally and economically efficient evaluation of RES. It supports new fields of study for university at all educational levels and enables the inclusion of new subjects specialized in the use of renewable energy carriers (REC) into the educational process.

Figure 2 Seminar room for 45 listeners

In the Research and Education Centre of Bioenergy (RECB), there is a solar system with three Bazicx 2.0 collectors and a photovoltaic system with three SF 150 panels installed (Figure 3). The solar system provides thermal water heating with a bilateral water tank which is used for the needs of the bioenergy centre. The electric energy which may be used, if necessary, for the operation of electric equipment in the centre is produced by the photovoltaic system and stored in 12V HAZE accumulator batteries (Fig. 4).

Figure 3 Solar and photovoltaic panels located on the roof of the centre building

Figure 4 Laboratory with solar and photovoltaic control system

4 Research and Education Activity of RECB

It is part of the workplace and predominantly deals with monitoring the operating parameters of the biogas station, on the basis of which a methodology for controlling the performance of the fermentation process was developed and limit values of basic parameters were determined, which best express the state of biogas production. At present, the performance of a biogas station is being continuously checked by measuring the temperature of the collected substrate, its initial pH, the dry matter content in the digestate – substrate, the concentration of biogenic elements C, H, N, S, O and the FOS/TAC parameter. The temperature of the substrate during fermentation is approximately 40°C and it should not fall below 20°C during transport for analysis. The substrate to be analyzed is collected in the second phase of the fermentation cycle, so its pH is usually in the range of 7.5 to 8.1. This value indicates that the anaerobic fermentation has passed into the methanogenic phase in which methane is formed as the main component of biogas. The dry matter content is expressed in % of the original weight

of the sample and its optimal value is 10 to 12%. At lower values the content of organic substances decreases and thus the specific volume production of biogas also decreases. The FOS/TAC method expresses the degree of anaerobic degradation process of the substrate which is given as a dimensionless number. This is the titration of the lower fatty acids, expressed in relation to the concentration of the total carbon, which determines the acid value and the moderating value of the substrate and thus the stability of the process may be best defined. Optimal FOS/TAC values are around 0.3 to 0.4. At these values biogas production is at maximum which represents approximately 55% of the methane content. Simultaneously, the recommendations and necessary measures were developed according to the measured FOS/TAC parameters during the process to ensure maximum efficiency of the fermentation process, see Table 1.

Table 1 Description of the fermentation process control based on FOS/TAC values

FOS/TAC	Process description	Recommendation
> 0,6	Very high biomass supply	Stop adding biomass
0,5 – 0,6	High biomass supply	Add less biomass
0,4 – 0,5	Loaded biomass	Monitoring of input biomass and its treatment
0,3 – 0,4	Biogas production is at maximum	Maintain input values
0,2 – 0,3	Biomass supply is low	Slowly increase biomass supply
< 0,2	Biomass supply too low	Rapidly increase the supply of biomass

The chemical-biological laboratory for testing the properties of biomass which is equipped with laboratory equipment in order to monitor operating parameters and increase the efficiency of the biogas station (BGS) may be divided into several parts according to the focus of their use as follows.

4.1 Sample preparation

Primary quartation of the samples taken is performed by quartation. The secondary preparation of the samples is provided by homogenizer on the Figure 5.

Figure 5 Grindomix GM 200 homogenizer by RETSCH

4.2 Macroelements analysis

The main building elements of biomass are carbon, nitrogen, hydrogen, sulphur and oxygen. These components are determined on the analyzer in Figure 6.

Figure 6 CHNS(O) analyzer Flash 2000 by Thermo Scientific

To assess lower organic proportions in digestate such as lactic, butyric, propionic, vinegar and formic acid, the analyzer in the Figure 7 is used.

4.3 Microelements analysis

The ZEEnit 700P atomic absorption spectrophotometer by Analytic Jena AG is used to

trace elements analysis, together with flame, hydride and electrothermal techniques for the determination of chemical elements in both liquid and solid samples (Figure 8).

Figure 7 Electrophoretic analyzer AE 102 by Villa Labeco

In case of liquid samples, the spectrophotometer shown in Figure 9 is used to determine Al, Ba, Cd, Co, Cu, Cr, Fe, Pb, Mn, Mo, Ni, polychlorinated biphenyls (PCBs), P, K, Se, Si, Ag and Zn. It may also be used for the determination of water, organic carbon, dissolved oxygen, phenols, PCBs, tannins, lignin, glucose. For the determination of mercury in solids and liquids the DMA-80 analyzer shown in Figure 10 is used.

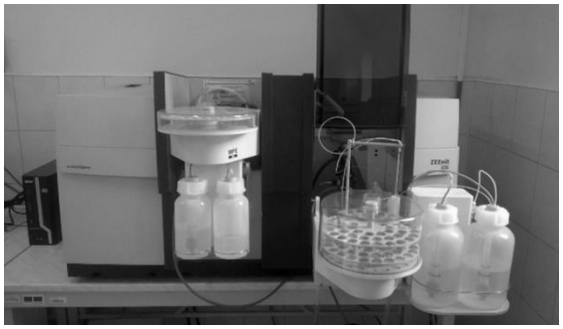

Figure 8 Atomic absorption spectrophotometer by Analytic Jena AG

5 Laboratory of Research of Liquid and Solid Biofuels

It deals with preparation and research of commonly used biofuels (Figure 11). Liquid biofuels include the production of biodiesel and bioethanol which may in principle be obtained in two ways. By fermenting biomass or pressing seeds and obtaining oils from them. The first method is more suitable for the hydrolytic decomposition of cellulose from biomass and the fermentation process. The second method is suitable for seeds with a high content of unsaturated fatty acids. For these purposes the laboratory is equipped with a large-capacity vacuum evaporator with a 20l distillation vessel by Heidolf Company for the preparation of bioethanol, and it is also equipped with pressing, filtering and mixing equipment by Farmet Company for obtaining oils from various types of phytomass.

Figure 9 Spectrophotometer SDR 2800 by Hach

Solid biofuels may be processed from dry biomass into pellets and briquettes. For the production of presswork in the form of pellets, the centre is equipped with a pelletizing line MGL 200 by Kovo Novak with a cutting pulverizer and conveyor. For the production of briquettes the BIOMASSER SOLO SET briquetting line with a cutter and a hygrometer is located in the centre. Pellets and briquettes are made from either wood sawdust or shavings without the addition of chemicals. Lignin found in wood acts as a binder, which at a high temperature caused by friction during their processing, turns into a plastic state. Recently, wood pellets have also been produced from fast-growing energy ground woods.

Figure 10 Direct Mercury Analyzer DMA-80 by MILLESTON

Figure 11 Laboratory of liquid and solid fuels with pressing, filtering and mixing equipment by Farmet Company

6 Conclusion

The reserves of individual energy sources in the territory of the Slovak Republic are constantly decreasing. Exclusively Renewable Energy Sources (RES) and especially biomass may play a significant role in maintaining or increasing them. It is confirmed that the use of RES as domestic energy sources increases to some extent the security and partial diversification of energy supply. The Slovak Republic has supported its determination to continue on the path of sustainable development by adopting the incorporation of basic principles into long-term strategic documents, such as the Energy Policy, The National Renewable Energy Action Plan, and the Concept of Energy Efficiency of the Slovak Republic. Slovakia's priority is to focus on key sectors of growth, and these are, in addition to environmental protection, energy efficiency and RES and also the support for research and development. The operation of Research and Education Centre of Bioenergy (RECB), as an innovative university workplace together with business practice, is focused on acquiring constantly new knowledge and research in the field of alternative energy sources and their utility in practice. It provides support for the educational process at all levels of education and promotes the use of new technologies on the basis of Renewable Energy Carriers (REC) in practice.

The reference list

[1] Ministry of Economy of the Slovak Republic. National renewable energy action plan, Bratislava, 2010, [Online], Available: http://www.rokovania.sk, [17 Feb 2020].

[2] JARÁBEK, M., LUNKIN, V.: *Energy policy of The Slovak Republic.* In: Conference Energy Efficiency until 2020, December 9th 2014 in Trnava, [Online], Available: https://www.siea.sk/materials/files/poradenstvo/aktuality/2014/energeticka_efektivnost_trnava/, [20 Jan 2020].

[3] Ministry of Agriculture and Rural Development of the Slovak Republic. *Report on agriculture and food in The Slovak Republic for 2017* (Green Report), National Food and Agricultural Centre – Research Institute of Agricultural and Food Economics, Bratislava, 2018.

[4] Ministry of Economy of the Slovak Republic. Energy Politics of The Slovak Republic, Bratislava, 2014, [Online], Available: http://www.rokovania.sk, [17 Feb 2020].

[5] Ministry of Economy of the Slovak Republic. Energy Efficiency Action Plan of The Slovak Republic for 2014 – 2016 with a view to 2020 Bratislava: ME SR, 2014, [Online], Available: http://www.rokovania.sk, [20 Jan 2020].

[6] Slovak Environment Agency, Ministry of Environment of the Slovak Republic, Department of sustainable environmental development. *AGENDA 21(CSD 2014)*, Bratislava, 2015. [Online]. Available: https://www.minzp.sk/files/dokumenty/ agenda21-sk.pdf [21 Jan 2020].

[7] Ministry of Education, Science, Research And Sport of the Slovak Republic. Research Agency. Research and Innovation Strategy for Smart Specialisation of the Slovak Republic (RIS3 SK) Bratislava, 2013, [Online]. Available at: http://www.vyskumnaagentura.sk/sk/o-nas/dokumenty/send/8-strategia-vyskumu-a-inovacii-ris3, [18 Feb 2020].

[8] Internal Regulations of The University of Economics. Organisation Rules of the Research and Education Centre of Bioenergy of The University of Economics in Bratislava – Kapušany workplace Bratislava, EU BA, 2018, [Online], Available: https://euba.sk/www_write/files/SK/docs/vnutorne-predpisy/2018/op_vvcb_kapusany_2018.pdf, [25 Jul 2019]

Acknowledgement

This article was created through the implementation of the project New technologies for energy environmental and economically efficient biomass evaluation, supported by the Operational Programme Research and Development funded by the EuropeanRegional Development Fund (ITMS code: 26220220063).

Advances in Thermal Processes and Energy Transformation
Volume 3, 2020, Siko01, pp. 71-74
ISSN 2585-9102

Analysis of Resistance of Clad Composite of Structural Steel and Tombac to Stress at Elevated Temperature

Kamil Sikora[1]

[1]*VÍTKOVICE ÚAM a.s., Ruská 2887/101 Ostrava, Czech Republic, E-mail: kamil.sikora@vitkovice.cz*

Category : Original Scientific Paper
Received : 24 October 2020 / Revised: 30 October 2020 / Accepted: 31 October 2020

Keywords : plating; rolling; steel; tombak

Abstract : Technological operations, where the temperature gradient significantly affects the thermal expansion of the material, require care in the choice of thermal stress with respect to the material used. A high temperature gradient can result in an increase in thermal stresses, which can result in plastic deformation of the material or even its failure. Clad materials are generally very sensitive to thermal stress. Especially if it is a composite material composed of layers with very different coefficients of thermal conductivity and thermal expansion, in our case structural steel and tombac. The aim of this study is to use the finite element method to simulate the maximum allowable thermal stress of a rolled clad composite composed of layers of tombac (CuZn90/10) and a core of structural steel S235JR + N, when there is no plastic deformation.

Citation: Sikora Kamil: Analysis of Resistance of Clad Composite of Structural Steel and Tombac to Stress at Elevated Temperature, Advance in Thermal Processes and Energy Transformation, Volume 3, No.3 (2020), pp. 71-74, ISSN 2585-9102

1 Introduction

The subject of the research project was the development of an innovative GMCS (Gilding Metal Clad Steel) production technology, which is described in this introductory chapter. GMCS production technology is a partial part of the complex technology of production of sheets and strips from Cu and CuZn alloys. The design of GMCS production technology is based on the conclusions of tests and development activities and contains basic procedures that must be subsequently modified and fine-tuned within the production process. The aim was to develop and verify a production technology in which brass plates (Ms90, CuZn10) and a steel core are joined. The resulting sheet should have a thickness of 1 mm after cold rolling.

The preparation of GMCS cartridges (packets) includes all activities leading to the production (cold) of the output product or. GMCS, which is the input material for the subsequent hot rolling technology on the DUO reverse rolling mill. The GMCS cartridge is a package of three layers of sheets wrapped and enclosed in a protective steel package.

The individual layers are stored in a protective packaging as follows:

• Bottom layer - sheet CuZn90/10 (Tombac).

• Middle layer - Steel block.

• Top layer - sheet metal CuZn90/10 (Tombac).

GMCS preparation includes the following basic activities:

a) one-sided surface grinding of CuZn90/10 sheets on a grinding machine,

b) blasting of steel blocks on a blasting machine,

c) cutting and pre-bending of the protective steel casing on sheet metal shears and a manual sheet metal bender,

d) application of separating coating,

e) storage of individual layers in a protective package, including its packaging and sealing on a packaging machine.

The protective cover of the GMCS cartridge is used to:

• As protection of CuZn90/10 sheets (tombac) when heated in a heating furnace (step furnace) to a temperature of 930-960°C (melting temperature CuZn90/10 is 1025-1045°C)

• As a connecting element, preventing the individual layers from shifting before the connection of the steel block to the tombac sheets after the first removal during hot rolling on the DUO rolling mill. The following image is an illustrative photograph of a rolled GMCS sheet.

1.1 Protective cover

The protective cover of the GMCS cartridge serves:

• As protection of CuZn90 / 10 sheets (tombac) when heated in a heating furnace (step furnace) to a temperature of 930-960°C.

• As a connecting element, preventing the individual layers from shifting before the connection of the steel block to the tombac plates after the first resp. the second removal during hot rolling on a DUO rolling mill.

Requirements for chemical composition, mechanical properties resp. other requirements for see above cladding materials (Chapter 2.1, indent 1) and 2)), are defined in DEF STAN 95-11 / Issue.

Figure 1 is an illustrative photograph of a rolled GMCS sheet. This is an innovative technology for the production of ammunition for firearms for military purposes, therefore the detailed specification is not public.

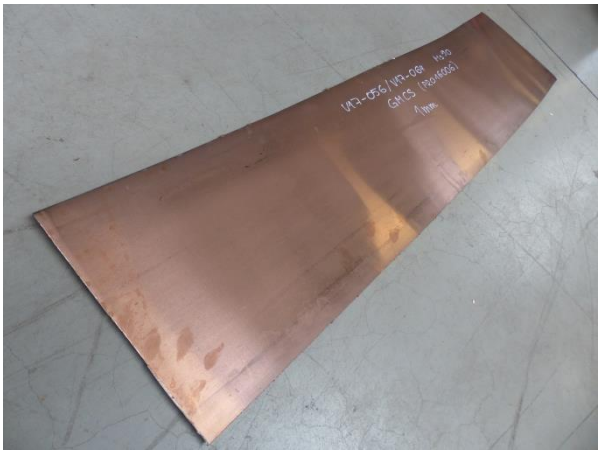

Figure 1 Photo GMCS plate

Based on previous operations, the final forming operation of the composite will take place - cold rolling. As it is a technology that combines several different technological processes, the resulting product is subjected to mechanical tests, which are preceded by mathematical analyzes.

2 Analysis of resistance to thermal stress

The presented analysis deals with the resistance of clad material made of structural steel S235JR + N and tombac CuZn90/10 to the effect of elevated temperature. The material is in the annealed state after cold rolling. The composite material consists of two 0.1 mm thick top layers of tombac and a 0.8 mm thick core of structural steel (Figure 1). The total thickness of the clad material is thus 1 mm. Due to the very different thermal expansion, it is necessary to determine the maximum temperature at which there is no plastic deformation due to thermal stresses. The finite element method was used for the determination. The computational model was performed in 3D SW ANSYS.

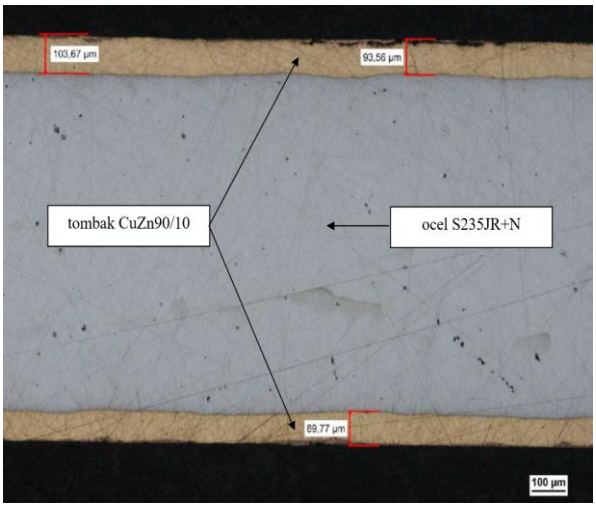

Figure 2 Image of metallographic cut of clad material with indication of thickness of rolled layers

3 FE simulation

The computational model consists of twenty-node quadratic elements SOLID186 (Figure 2). For the purpose of calculating the thermal stress alone, a multiple symmetric boundary condition was preferably chosen (Figure 3). The temperature is entered unitally. The problem is solved as stationary, because test calculations with a non-stationary temperature field due to the high thermal conductivity of both metallic materials are meaningless.

The material behavior model is homogeneous isotropic nonlinearly elastic. The nonlinear dependence of all material properties is the temperature dependence, where the required intermediate values are obtained by interpolation. The mechanical-physical properties of the CuZn90/10 tombac could not be obtained for higher temperatures. For this reason, the properties of pure copper were used, taking into account the ratio of the mechanical properties of pure copper and tombac at a temperature of 20°C. Used mechanical-physical properties of steel, (tombac) are listed in Table 1, resp. in Table 2. Most values are drawn from the literature [1] and [2]. Unfortunately, the possible strengthening of steel or tombac cannot be included in the calculation model, because the changes of mechanical-physical properties of the finished clad

material after the last technological operation of the production of clad material are not known. Likewise, small deviations of the mechanical properties in the rolling direction and perpendicular to the rolling direction can be expected. Since the technological process also includes rolling at elevated temperatures, it can be assumed that the residual stresses are at most at the level of the yield strength at a temperature equal to the rolling temperature. Such a residual stress would be insignificantly small. The insignificance of residual stresses is also supported by the fact that the finished clad semi-finished products do not show any deformation, such as surface undulation.

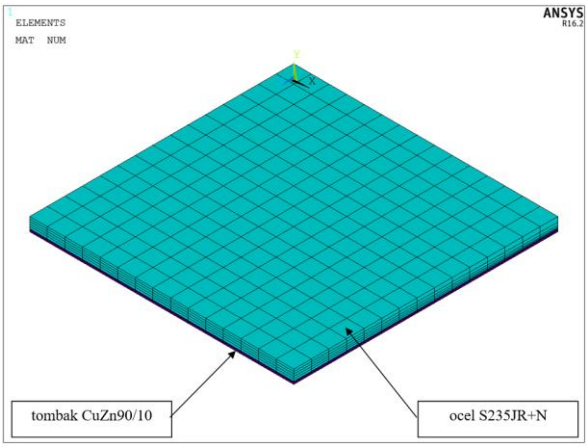

Figure 3 Computational model - finite element network

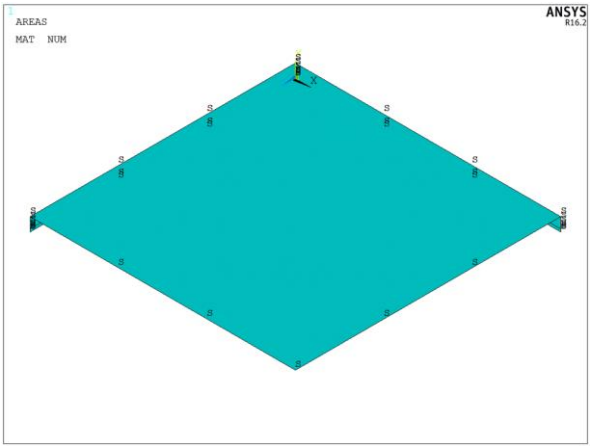

Figure 4 Computational model - symmetric boundary conditions

The network of finite elements and boundary conditions of the mathematical model were adapted to the dimensions of the actual product and the predicted type of load.

Table 1 Mechanical properties of steel S235JR + N

					μ = 0,30 [-], ρ = 7850 [kg/m³]
T [°C]	E [MPa]	α.10⁶ [1/K]	λ [W/m.K]	c [J/kg.K]	Re [MPa]
20	200000	11,5	51,7	472	196
100	195000	11,9	51,1	496	196
200	190000	12,5	48,5	525	196
300	180000	13,1	44,4	565	157
350	175000	13,4	43,5	586	135

Table 2 Mechanical properties of tombac CuZn90/10

					μ = 0,34 [-], ρ = 8960 [kg/m³]
T [°C]	E [MPa]	α.10⁶ [1/K]	λ [W/m.K]	c [J/kg.K]	Re [MPa]
20	129800	15,4	15,3	383	211
100	125500	16,2	16,3	398	205
200	120000	16,9	17,6	408	182
300	114500	17,7	18,9	417	126
350	112000	18,1	19,5	421	95

The mechanical properties of both investigated materials show an indirect relationship between the modulus of elasticity and the longitudinal expansion.

4 Results

The result of the computational modeling for the temperature of 350°C is shown in the form of a stress field. In Figure 5-7 the reduced stress according to the Tresca condition in MPa is presented. The results of all calculations are summarized in the form of a graph in Fig. 8. The stresses *σINT*_tombak are calculated for a given temperature, *σY*_tombak represents the yield strength of the tombac for a given temperature, σY_steel represents the yield strength of the steel for a given temperature. In all standards, a limit is set for a simple membrane stress, usually 2/3 of the yield strength for a given temperature. This limit ensures safety against reaching the plastic deformation limit state. The voltages *σ*_tombak represent the limit for a given temperature at the tombac. The stresses *σ*_steel represent the limit for a given temperature for steel.

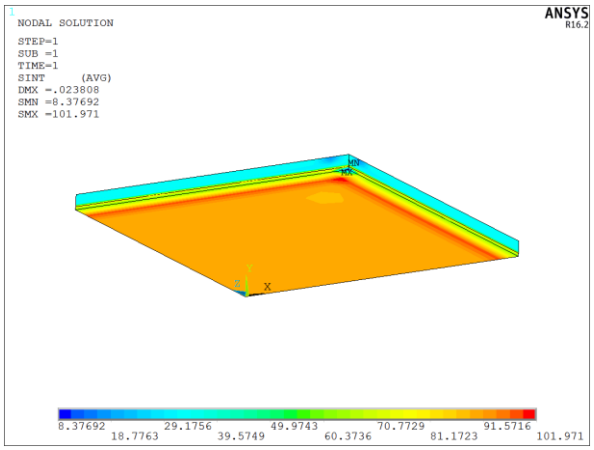

Figure 5 Stress according to Tresca condition at 150°C

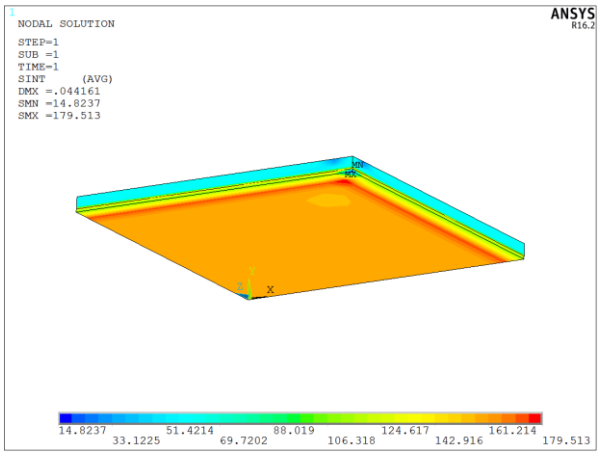

Figure 6 Stress according to Tresca condition at 250°C

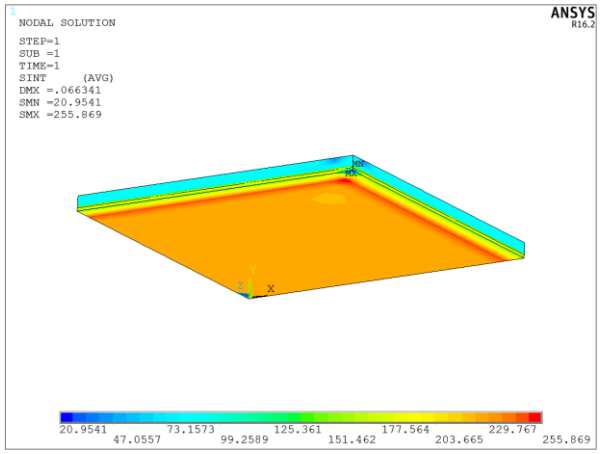

Figure 7 Stress according to Tresca condition at 350°C

On the color scale of Figure 5-7 we see the difference in the stress field of the individual layers, declared above in the longitudinal expansion of both materials in Tables 1 and 2 (column 3). The modulus of elasticity is thus a determining parameter for the prediction of plastic deformation.

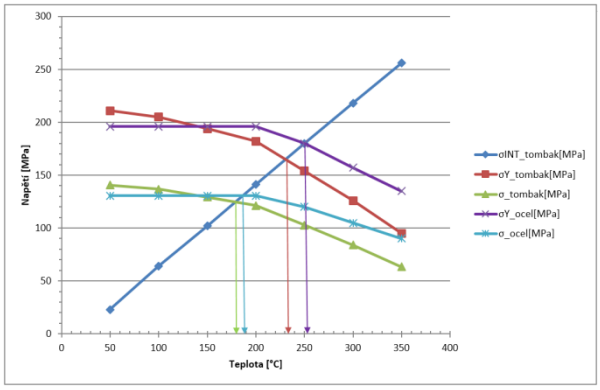

Figure 8 Summary of results

The results of mathematical modeling show that the yield strength and safety limits do not deviate from the predicted values declared by the standard. Based on a mathematical model, plastic deformation at the joint of both materials should occur after the temperature exceeds 250°C.

5 Concusion

The computational analysis shows that the clad material made of steel S235JR + N with a thickness of 0.8 mm with double-sided rolled tombac CuZn90/10 with a thickness of 0.1 mm is not suitable for exposure to higher than about 250 °C. Above this temperature, due to the different thermal expansion of steel and tombac, plastic deformation of the clad material as a whole is likely to occur. At temperatures up to approx. 230°C, no plastic layer is deformed. When exposed to temperatures up to approx. 190°C, the clad material has only 2/3 of the yield strength exhausted, which is the limit value for the membrane stress in commonly used standards for calculations and assessment of vessels and structures. Temperatures up to 180 °C appear to be the most suitable from the point of view of the production of clad material, which was the subject of computational modeling. At the indicated temperature, the yield strength of the tombac layer is 1/3 of the yield strength value for the given temperature. A temperature higher than 230°C can lead to plastic deformation associated with a permanent change in shape. At the same time, it is desirable that the clad material is not exposed to a temperature higher than 230°C before the last technological step.

References

[1] HEWITT, G.F.: *Heat excharger design handbook*, Begell House, Inc., New York, Wallington, 1998.

[2] NTD ASI – II – 2017 Normativně technická dokumentace A.S.I. Charakteristiky materiálu pro zařízení a potrubí JE typu VVER, Sekce II, Praha a Brno 2017.

Advances in Thermal Processes and Energy Transformation
Volume 3, 2020, Strb01, pp. 75-80
ISSN 2585-9102

Design of the Minimal Length Nozzle for Ejector Cooling System by Using Method of Characteristics

Dominik Štrba[1] ● Peter Mlynár[2] ● Michal Masaryk[3]● Georgios Manganos[4]

[1]*Institut of Energy Machinery, Faculty of Mechanical Engineering, Slovak University of Technology, Námestie slobody 17,812 31 Bratislava, Slovakia, dominik.strba@tuba.sk*
[2]*Institut of Energy Machinery, Faculty of Mechanical Engineering, Slovak University of Technology, Námestie slobody 17,812 31 Bratislava, Slovakia, peter.mlynar@stuba.sk*
[3]*Institut of Energy Machinery, Faculty of Mechanical Engineering, Slovak University of Technology, Námestie slobody 17,812 31 Bratislava, Slovakia, michal.masaryk@stuba.sk*
[4]*Institut of Energy Machinery, Faculty of Mechanical Engineering, Slovak University of Technology, Námestie slobody 17,812 31 Bratislava, Slovakia, georgios.manganos@stuba.sk*

Category: Original Scientific Paper
Received : 21 October 2020 / Revised: 29 October 2020 / Accepted:30 October 2020

Keywords: ejector, ejector cooling system (ECS), minimal length nozzle (MLN), method of characteristics (MOC)

Abstract: In this paper will be presented design of the minimal length nozzle (MLN) used for ejector cooling system (ECS). Working fluid in this circuit is water (steam). Correct and precious design of the nozzle is crucial for the right operation of the ECS system. For design of MLN was used method of characteristics (MOC), which was explained in the article. In the end there was shown program made for calculation of the MLN in Graphical User Interface (GUI) of open source program Scilab.

Citation: Štrba Dominik, Mlynár Peter, Masaryk Michal, Manganos Georgios: Design of the Minimal Length Nozzle for Ejector Cooling System by Using Method of Characteristics, Advance in Thermal Processes and Energy Transformation, Volume 3, No.3, (2020), p. 75-80, ISSN 2585-9102

1 Introduction

Research of our team is focused on the ejector cooling systems (ECS) in combination with Fresnel solar collector. The ECS system runs on the heat. As working fluid was used water. Advantages of the water as a fluid are that water is cheap and available. It is also easy to work with it and it is not dangerous for human health. Another advantage of water is ecological aspect, that means water has no impact on environment, its impact on ozone layer is none (ODP=0) and also has no impact on global warming (GWP=0) [1]. Main disadvantage is that if evaporating temperature in evaporator is set for t_e=3°C, absolute pressure for liquid water to evaporate is p_e=758Pa, which is deep vacuum. For this reason is needed to create really precious nozzle which can ensure this level of the absolute pressure. In the past were used conical nozzles, which do not take in action Prandtl-Meyer expansion. The flow is not regulated for elimination of radial component of the velocity. Price and manufacturability is the reason why was this type used mostly in the past [2]. In this article will be shown

how to design parabolic nozzle which take into account Prandtl-Meyer expansion.

2 Theoretical background

2.1 Ejector cooling system (ECS)

ECS creates vacuum in ejector which is non-moving part using heat for operation. Primary steam is created in the generator.

Nomenclature

A	starting point
COP	coefficient of performance
D	diameter [mm]
ECS	ejector cooling system
GWP	global warming potential
M	Mach number [-]
MLN	minimal length nozzle
MOC	method of characteristics
a	speed of sound [m/s]
n	number of characteristic lines [pcs]
p	pressure [Pa]
u	velocity [m/s]
v	velocity [m/s]
t	temperature [°C]
Greek symbols	
α	angle [°]
β	angle [°]
θ	inclination angle [°]
κ	isentropic coefficient [-]
μ	expansion angle [°]
ν	Prandtl-Meyer angle [°]
Subscripts	
1,2,3	points of the grid
e	exit of the nozzle
*	critical section

A primary steam enters into the ejector, where is expanded into higher velocity because of the convergent part of the nozzle, in place of the critical diameter *D** of the nozzle reached the Mach number, where *M*=1*, after critical diameter there is divergent part of the nozzle, where is flow accelerated even more. This accelerated flow gets out of nozzle with supersonic velocity, vacuum and suction effect are obtained for secondary steam from evaporator. In the suction chamber are primary and secondary flow sucked and in mixing chamber are mixed. In the exit of the diffusor mixed flow get out of ejector and enters into the condenser with needed condensing pressure for condensation of the steam to the liquid. From condenser is working fluid divided into two streams, first is coming back to the evaporator through expansion valve and second one is going to the generator where is primary steam created.

In comparison with a compressor cooling system, the ECS system does not have any moving or rotating parts needed for compression of the refrigerant. In the ECS lubrication is not needed because the pressure increase is made by a stationary ejector. Also there are no problems with compression in high temperature conditions. One of the biggest advantages of these systems is that when energy is most needed for cooling there is the greatest amount of solar energy. Electricity consumption is in this case lower than in the compression cooling system because here electricity is used only for pumps and they consume only about 5-10 % of the electricity used by a compressor. It means that in the ejector cooling system cooling capacity is created by the ejector and a pump unlike in the compressor cooling system, where only a compressor is used, with high electricity consumption. Another advantage of the ejector cooling system is that is a renewable source of energy [1].

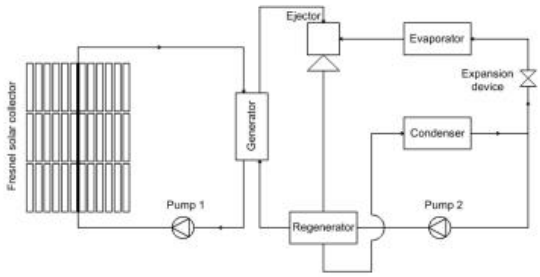

Figure 1 Ejector cooling system with Fresnel solar collector

The main disadvantage of the ECS is a low value of COP coefficient (Coefficient of performance). For this reason solar heat or waste heat is used for driving this system. It's not economical to produce heat directly for creating steam to power the cooling system [3].

2.2 Method of characteristics (MOC)

This method is used for finding geometry of the divergent part of the sonic nozzle with minimal length (MLN). Consider steady, two-dimensional, adiabatic, irrotational supersonic flow. Replace the two-dimensional current field with a rectangular grid [4, 5]. At these points, the parameters are either known, given the geometry or are subject to numerical calculation. If there are no particles in the current field that perform a vortex motion than ($v \times \nabla = 0$), velocity could be written in the form of a scalar field:

$$\bar{v} = \nabla\phi \qquad (1)$$

Differential equation of continuity valid for steady state flow:

$$\nabla(\rho\vec{v}) = \frac{\partial}{\partial x}(\rho\phi_x) + \frac{\partial}{\partial y}(\rho\phi_y) = 0 \qquad (2)$$

$$\rho(\phi_{xx} + \phi_{yy}) + \phi_x\frac{\partial\rho}{\partial x} + \phi_y\frac{\partial\rho}{\partial y} = 0 \qquad (3)$$

The law of conservation of momentum in differential form is as follows:

$$dp = -\rho\frac{d(\phi_x^2+\phi_y^2)}{2} \qquad (4)$$

The change in the density of the medium in the case of isentropic flow can be described by a change in the pressure and speed of sound:

$$dp = \frac{dp}{a^2} - \frac{\rho}{a^2}d\left(\frac{\phi_x^2}{2} + \frac{\phi_y^2}{2}\right) \qquad (5)$$

After expressing the density gradient in the x and y directions, the partial differential equation were substitute into the relation and replace it with the velocity components *u* and *v* of the partial derivatives of the scalar fields, equation then is:

$$\left(1-\frac{u^2}{a^2}\right)\frac{\partial^2\phi}{\partial x^2} - \frac{2uv}{a^2}\frac{\partial^2\phi}{\partial x\partial y} + \left(1-\frac{v^2}{a^2}\right)\frac{\partial^2\phi}{\partial y^2} = 0 \qquad (6)$$

If $u = \frac{\partial\emptyset}{\partial x}$ and $v = \frac{\partial\emptyset}{\partial y}$, after derivation there is

$$\mathrm{du} = d\left(\frac{\partial\phi}{\partial x}\right) = \frac{\partial^2\phi}{\partial x^2}dx + \frac{\partial^2\phi}{\partial x\partial y}dy \qquad (7)$$

$$\mathrm{dv} = d\left(\frac{\partial\phi}{\partial y}\right) = \frac{\partial^2\phi}{\partial y^2}dy + \frac{\partial^2\phi}{\partial x\partial y}dx \qquad (8)$$

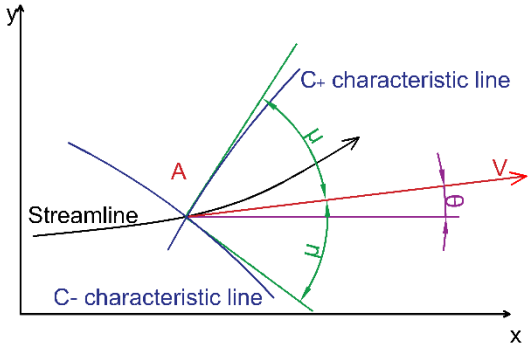

Figure 2 Illustration of left-running and right-running characteristic lines

In equations (6) – (8) there is 3 unknown, system of 3 unknown is calculated by Cramer's rule.

$$\frac{\partial^2\phi}{\partial x\partial y}dx = \frac{\begin{vmatrix} 1-\frac{u^2}{a^2} & 0 & 1-\frac{v^2}{a^2} \\ dx & du & 0 \\ 0 & dv & dy \end{vmatrix}}{\begin{vmatrix} 1-\frac{u^2}{a^2} & \frac{-2uv}{a^2} & 1-\frac{v^2}{a^2} \\ dx & dy & 0 \\ 0 & dx & dy \end{vmatrix}} \qquad (9)$$

A graphical interpretation of matrix from Equation (9) is show on the Figure 2. Point A is nodal point of the grid of flow field. If the ratio *dx/dy* is correctly chosen, determinant of denominator could be equal to zero. It means in the flow field exists characteristic line, after which the left side of the Equation (6) will be indefinite. According to [6] is this direction described with this equation:

$$\left(\frac{dx}{dy}\right)_{char} = \tan(\theta \pm \mu) \qquad (10)$$

This characteristic lines are equivalent of expanse lines arising from super and hypersonic flow. For simplicity, these lines are considered for straight lines.

Characteristic lines could be 2 types lying at an angle:

1. $\boldsymbol{\mu - \theta}$ are left-running characteristics, where $\boldsymbol{\theta + \nu(M) = const}$.
2. $\boldsymbol{\mu + \theta}$ are right-running characteristics, where $\boldsymbol{\theta - \nu(M) = const}$.

If there is known any of the parameters $\boldsymbol{\theta, \nu, M}$ of starting point is possible to calculate every point of the grid using compatibily equations [6 - 9]. Starting point is place, where flow reached the sonic speed and its Mach number is equal to 1. This point is called critical and its diameter is called critical diameter *D**.

3 Computation of the geometry of the minimal length nozzle (MLN)

Points of the grid are divided into the two groups, depends on the position and the method of finding:

1. Internal points of flow field
2. Wall points

Characteristic lines are divided into 3 groups:

1. Left-running characteristics from starting point (where Mach number is M=1)
2. Characteristic lines reflected from the axis
3. Characteristic lines captured by the wall

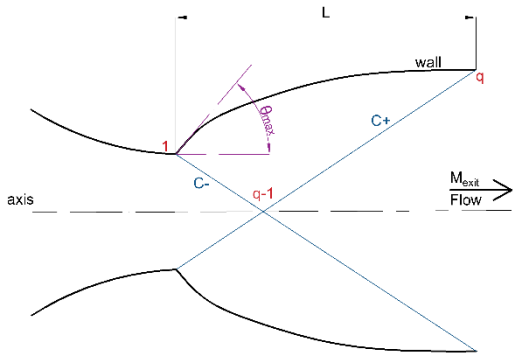

Figure 3 Contour of the MLN

Nozzle is axis symmetrical. Right-running and left-running characteristics starts from starting point, reflected from the axis and captured in the wall. Calculated grid is defined by the number and position of the intersections created during interaction of two characteristic lines. Every point is clearly characterized by θ and ν(M).

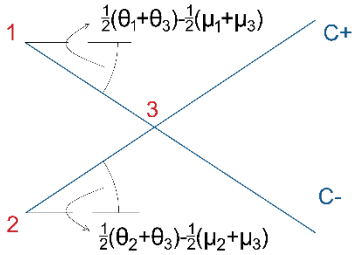

Figure 4 Approximation of characteristics by straight lines

Inclination angle of the first left-running characteristic is the first step for calculation of final geometry of the MLN. According to Prandtl-Meyer expansion theory, inclination angle in point 1 is equal to:

$$\theta_{max} = \frac{\nu_e}{2} \qquad (11)$$

Point 2 is located on this left-running characteristic and also on the axis of the nozzle, inclination angle of this point is equal to 0°.

Point 3 is located on the intersection of two characteristics. Coordinates of this point are calculated by using these equations:

$$x_i = \frac{(y_1 - x_1 \tan\alpha) - (y_1 - 1 - x_{i-1} \tan\beta)}{\tan\beta - \tan\alpha} \qquad (12)$$

$$y_i = y_{i-1} + (x_i - x_{i-1}) \tan\beta \qquad (13)$$

$$\alpha = \frac{(\theta-\mu)_1 + (\theta-\mu)_i}{2} \qquad (14)$$

$$\beta = \frac{(\theta+\mu)_1 + (\theta+\mu)_i}{2} \qquad (15)$$

Mach number for the points of the grid are calculated by Prandtl-Meyer equation [7, 10]:

$$\nu(M) = \sqrt{\frac{\kappa+1}{\kappa-1}}\, atan \sqrt{\frac{\kappa+1}{\kappa-1}(M^2-1)} - atan\sqrt{(M^2-1)} \qquad (16)$$

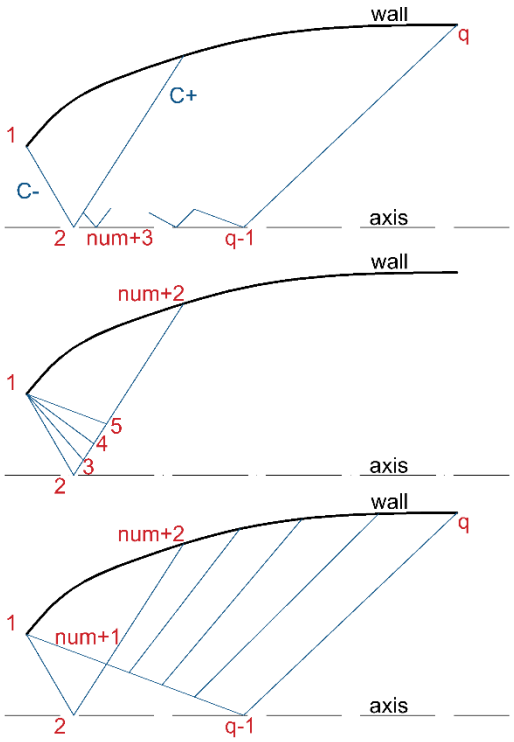

Figure 5 Different kinds of characteristic lines and points of the net

Vectors of the velocities in points which are located on the axis has only axial component, inclination angles of these points are equal to 0°. Coordinates of these points can be calculated as follow:

$$x_{num+3} = x_a \frac{y_{num+3} - y_a}{\tan\alpha} \qquad (17)$$

$$\alpha = \frac{(\theta-\mu)_a + (\theta-\mu)_{num+3}}{2} \qquad (18)$$

Internal points are created as intersections of right-running and left-running characteristics.

Wall points are used for final design of the supersonic minimal length nozzle. If there is more of the characteristic lines which starts from starting point [0,R*], the difference of the angle dθ is smaller and final contour of the nozzle is smoother. Coordinates of these points can be calculated as follow:

$$x_{num+2} = \frac{(y_1 - x_1 \tan\alpha) - (y_{num+1} - x_{num+1} \tan\beta)}{\tan\beta - \tan\alpha} \quad (19)$$

$$y_{num+2} = y_{num+1} + (x_{num+3} - x_{num+1}) \tan\beta \quad (20)$$

$$\alpha = \frac{\theta_1 + \theta_{num+2}}{2} \quad (21)$$

$$\beta = \frac{(\theta+\mu)_{num+1} + (\theta+\mu)_{num+2}}{2} \quad (22)$$

4 Program for calculation of geometry of the minimal length nozzle (MLN)

Equations from Chapter 3 where used for creating program for calculation of the contour of the MLN. This program was made in the Graphical User Interface (GUI) of the open source program Scilab. Program was made for steam as working medium. Main window and inputs are shown on Figure 6. Inputs needed for calculation of the final contour are:

- Inlet pressure p_{in} *[kPa]*
- Outlet pressure p_{ex} *[kPa]*
- Amount of the charact. lines *n [pcs]*
- Critical diameter of the nozzle *D* [mm]*
- Isentropic coefficient *κ[-]*

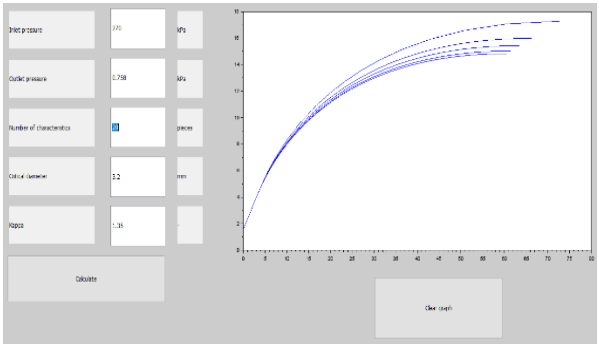

Figure 6 Graphical interface of the scilab program

As the output from the program there are [x, y, z] coordinates which can be used for creating the 3D model of the minimal length nozzle. As it shown in the Table 1, choice of the number of the characteristic lines is crucial. With increasing of number of characteristic lines, results are more precise but time needed for calculation increases exponential. For this reason, for two dimensional analysis is recommended to use minimal 50 characteristic lines.

Table 1 2D coordinates of the MLN as results from the program

No. of char.lines	x [mm]	y [mm]
5	109,09	24,97
10	82,81	19,35
20	72,67	17,27
30	68,86	16,50
40	66,33	15,99
50	64,62	15,65
60	63,52	15,43
70	62,62	15,25
80	61,52	15,03
90	61,44	15,02

With the results from the program was made 3D model of the MLN in program Autodesk Fusion 360, see Figure 7.

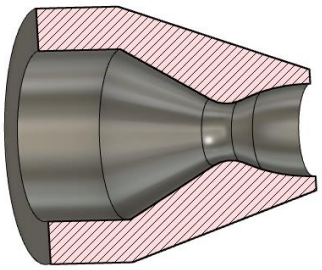

Figure 7 3D design of the minimal length nozzle

5 Conclusion

In this article was shown method for calculation contour of minimal length nozzle (MLN) used for ejector cooling system with steam as working fluid. For design of nozzle contour was used Method of Characteristics (MOC) in Graphical User Interface (GUI) in open source program Scilab. Next steps in research are to run the simulation for verifying the result from this calculation and after simulation to make experimental tests of the designed MLN.

The reference list

[1] PRIDASAWAS, W.: *Solar-Driven Refrigeration Systems with Focus on the Ejector Cycle*, Stockholm, 2006.

[2] VAVRO, K., PECIAR, M.: *Ejektory a injektory*, Bratislava, Nakladatel'stvo STU, 2011.

[3] CHAQING, L.: *Gas ejector modeling for design and analysis,* Texas, 2008.

[4] FUSZKO, Z.: *Návrh Lavalovej dýzy pre nadzvukové ejektory:* diplomová práca. Bratislava, 2014.

[5] FUSZKO, Z.: *Prúdenie v predradenom dvojstupňovom supersonickom ejektore*, Bratislava, 2018.

[6] ZUCKER, R.: *Fundamentals of gas dynamics.* Monterey: Department of Aeronautics and Astronautics, 1977.

[7] JANALIK, J., ÖSTLUND, J.: *Flow Processes in Rocket Nozzles with Focus on Flow Separation and Side-Loads,* Stockholm: Royal Inst. Of Technology, TRITA-MEK 202:09, 2002.

[8] ANDERSON, J.D.: (ed.) *Modern Compressible Flow: With Historical Perspective, 3rd Edition*, Quebecor World Fairfield, 2003.

[9] ANDERSON, J.D.: (ed.) *Fundamentals of Aerodynamics, 5th Edition*, R.R. Donnelley, 2010.

[9] LORD, T. W.: *A Theoretical Study of Annular Supersonic Nozzles.* London: Her Majesty's stationery office, Ministry of Aviation, 1961.